RSC Advances

ROYAL SOCIETY OF CHEMISTRY

www.rsc.org/advances

Journal Name

ARTICLE

Fabrication and evaluation of protein imprinted polymer based on magnetic halloysite nanotube

Received 00th January 20xx,
Accepted 00th January 20xx

DOI: 10.1039/x0xx00000x

www.rsc.org/

Xiaohong Zhu,[a] Hui Li,[a] Hui Zhou[b] and Shian Zhong[a*]

A novel protein imprinted polymer, which combined the surface imprinting technology and the magnetic halloysite nanotubes (MHNTs), was prepared for selective separation of template protein. In this work, MHNTs were synthesized through the coprecipitation method based on encapsulation of Fe_3O_4 nanoparticles in halloysite nanotubes. The surface of the MHNTs was modified with vinyl groups through reaction with 3-(methacryloyloxy)propyl trimethoxysilane. Subsequently, the modified MHNTs were used as support, N-isopropylacrylamide and methacrylic acid as bifunctional monomers, N,N'-methylene bisacrylamid as crosslinking agent, and ammonium persulphate and N,N,N',N'-tetramethylethylenediamine as initiators. The resulting polymer was named as MHNTs@BSA-MIP, which was characterized by transmission electron microscopy, Fourier transform infrared spectroscopy, X-ray diffraction, and vibrating sample magnetometry. The MHNTs@BSA-MIP exhibited high adsorption (48.4 mg/g), good selectivity, rapid kinetic binding (45 min), fast magnetic separation (10 s), and favorable reproducibility (relative standard deviation < 8% for batch-to-batch evaluation). The prepared MHNTs@BSA-MIP is suitable for separation and provides a significant reference for other proteins in proteomics.

1 Introduction

Recently, separation and enrichment of purified proteins have attracted considerable interest because of their increasing significance in various applications ranging from diagnostics to therapeutics. Traditionally, immobilized metal ion affinity chromatography,[1] aqueous two-phase systems,[2] or electrophoretic–electroosmotic focusing[3] can be used to separate proteins from cell debris or to purify proteins from other proteins. However, these techniques have several limitations such as poor stability, high cost, non-reusability, and complex operation technology. Therefore, developing a new method for protein separation is of great importance.

Molecular imprinting technology is promising strategy for rapid and inexpensive production of biomimetic materials, which can generate synthetic materials with specific recognition sites.[4, 5] Compared with its biological counterparts, molecularly imprinted polymer (MIP) displays significant advantages, including high mechanical properties, chemical stability, easy preparation,[6] potential reusability, and low manufacturing cost.[7] Nevertheless, when regard to biological macromolecule imprinting, some inherent limitations exist, such as insolubility in water, poor mass transfer, and low integrity.[8] In order to overcome these limitations, several strategies, including the use of metal-coordination polymerization,[9, 10] epitope approach,[11-13] and surface imprinting,[14-22] have been employed in protein imprinting.

Among these methods, surface imprinting with supporter has become an effective solution to achieve excellent recognition and adsorption, by which recognition sites were formed on the material surface. Different supporting substrates such as silica nanoparticles,[23-25] carbon nanotubes (CNTs),[26, 27] Fe_3O_4,[28, 29] and oxidized metal complex nanoparticles, have been developed to prepare MIP. Great efforts have been performed to combine CNTs with the MIP. Chen et al. synthesized a novel MIP based on modified CNTs by using bovine serum albumin (BSA) as the template, which exhibited high sensitivity, and good reproducibility.[30] Huang and his co-workers combined the advantages of CNT–AuNP composites and chitosan to design a disposable and sensitive MIP for tyramine detection.[31]

However, CNTs show poor dispersibility in organic phase or aqueous phase, and thus modification is necessary prior to use. By contrast, halloysite nanotubes (HNTs) disperse well in water. HNTs are aluminosilicate clay mineral with a 1:1 Al:Si ratio and ideal chemical formula of $Al_2Si_2O_5(OH)_4 \cdot nH_2O$, which were chemically similar to kaolin, but differ in having a hollow tubular structure rather than a stacked plate-like structure.[32, 33] HNTs exhibit potential application owing to their gibbsite octahedral sheet aluminum (innermost) and silicate (outermost) surfaces, which allow different chemical reactions

[a] School of Chemistry and Chemical Engineering, Central South University, Changsha 410083, China Tel: +86 13107210768 ,Email address: zhongshian@aliyun.com
[b] *The affiliated cancer Hospital of Xiangya School of Medicine, Central South University, Changsha 410013, China*

in the interior and exterior surfaces. Similar to most natural materials, the sizes of HNTs vary between 500 and 1000 nm in length and 10-150 nm in inner diameter depending on the deposits. HNTs are environmentally friendly, and available at low cost. In addition, large reserves of HNTs are found in China. [34] HNTs have unique properties including non-swelling, large surface area and abundant hydroxyl groups. Thus, the combination of Fe_3O_4 and HNTs can form the magnetic HNTs (MHNTs),[35, 36] which can be applied in adsorption technology. Pan and co-workers used MHNTs combined with MIP as sorbent for solid-phase extraction and separation of 2,4,6-trichlorophenol from environmental water samples.[37] Our group also fabricated the MIP on the surface of MHNTs for recognition of herbicides.[38] In these previous studies, low-molecular weight compounds were used as template molecules. However, no reports had described a preparation of protein-imprinted polymer on the surface of MHNTs. Therefore, we developed a new preparation method for covering MHNTs with MIP, combining both surface molecular imprinting technology and nanotechnology.

In this study, a facile and versatile approach was developed to prepare MIP based on modified MHNTs. First, MHNTs were fabricated by a straightforward and effective coprecipitation method. Then, a vinyl group was introduced on the surface of MHNTs to graft MIP onto MHNTs. Subsequently, MHNTs@BSA-MIP was synthesized by a precipitation polymerization method, in which the modified MHNTs were used as the support matrix, N-isopropylacrylamide (NIPAM) and methacrylic acid (MAA) as the co-monomers, N,N'-methylene bisacrylamide (BIS) as the crosslinking agent. Characterization and performance evaluation of the prepared MHNTs@BSA-MIP were conducted. The MHNTs@BSA-MIP can selectively recognize the template protein in a complex matrix and it possesses numerous imprinted cavities within the polymer network owing to the high surface-to-volume ratio of MHNTs.

2 Experimental

2.1. Chemicals and reagents

All chemicals were of analytical reagent grade. Double-distilled water was used in the experiments. The proteins were as follows: bovine serum albumin （BSA, MW =68 kDa, pI =4.9）, lysozyme (Lyz, MW=13.4 kDa, pI=11.2), ovalbumin (OVA, MW=43.0 kDa, pI=4.7), and trypsin from bovine pancreas (Try, MW=12.6 kDa, pI=7.8). All proteins were purchased from Energy Chemical.

HNTs were supplied by Zhengzhou Jinyangguang Co., Ltd. (Henan, China). $FeCl_3{\cdot}6H_2O$, $FeCl_2{\cdot}4H_2O$, and 3-methacryloxypropyltrimethoxysilane (MPTES) were supplied by Sinopharm Chemical Reagent Co., Ltd. (Shanghai, China). NIPAM, MAA, BIS, ammonium persulphate (APS), and N,N,N',N'-tetramethylethylenediamine (TEMED) were purchased from Aladdin Company (Shanghai ,China). Sodium dodecyl sulfate (SDS) was purchased from Tianjin Chemical Reagents Co., Ltd.

2.2. Apparatus and conditions

UV-vis spectra were obtained using a UV-2450 Spectrophotometer (Shimadzu, Japan). Fourier transform infrared (FT-IR) spectroscopy was employed to obtain infrared spectra (Nicolet, America). The samples were prepared by mixing the products with KBr and pressing into a compact pellet. Morphology and size distribution of the MHNTs and MHNT@MIP were investigated using transmission electron microscopy (TEM, JEM-2100F, Japan) at 20.0 kV. Particle phases were characterized using X-ray diffraction (XRD, Rigaku D/max22500 XRD) with Cu Ka radiation (Rigaku Ltd., Japan). Magnetic properties were determined using vibrating sample magnetometry (VSM, Lake Shore Ltd.) at room temperature.

2.3 Preparation of MHNTs

MHNTs were synthesized according to our previous reported method. Crude HNTs were sieved and then dried at 100 °C in an oven for 12 h. HNTs weighing 0.5 g were briefly dispersed in 150 mL of deionized water by sonication for 15 min, and then 1.30 g of $FeCl_3{\cdot}6H_2O$ and 0.48 g of $FeCl_2{\cdot}4H_2O$ were added. The mixture was stirred for 10 min at 60 °C in N_2 atmosphere. Subsequently, 10 mL of ammonia solution was added dropwise into the mixture solution. The addition of the base to the Fe^{2+}/Fe^{3+} salt solution resulted in the immediate formation of black precipitates of MHNTs. Then, the resulting reaction mixture was aged for 4 h at 70 °C. The MHNTs were separated by an external magnetic field and washed for three times sequentially with water and ethanol. Finally, the MHNTs were dried in vacuum at 60 °C.

2.4 Preparation of vinyl modified MHNTs

MPTES, as a silane coupling agent, was used to prepare the functionalized MHNTs (MHNTs@C=C). MHNTs weighing 250 mg were dispersed in 15 mL of anhydrous toluene in a three-necked flask. Then 3 mL of MPTES was added into the solution. The mixture was allowed to react for 24 h at 90 °C under constant stirring under an N_2 atmosphere. After cooling to room temperature, the resultant was washed sequentially with water and ethanol. The MHNTs@C=C was collected by an external magnetic field and dried in vacuum at 60 °C.

2.5 Preparation of MHNTs@BSA-MIP and MHNTs@ NIP

MHNTs@BSA-MIP was obtained by the following method: 25.0 mg of BSA was dissolved in 20.0 mL of 0.1 mol/L phosphate buffer (pH 6.98) in a three-necked round-bottomed flask, and then 84.8 mg of NIPAM and 21.5 mg of MAA as co-monomers were added. The resulting mixture was dispersed homogeneously and shook for 5 h in the dark at room temperature to allow self-assembly. Subsequently, 200 mg of MHNTs, 7.8 mg of BIS, 10 mg of APS, and 10 μL of TEMED were added to the self-assembly solution. The solution was deoxygenated by purging with nitrogen for 15 min. The reaction was allowed to proceed at 35 °C for 24 h under mechanical stirring. Afterward, the products were separated

by an external magnetic field and then repeatedly rinsed with distilled water to remove unreacted monomers and crosslinker. Then, the template protein was eluted with SDS-acetic acid (10% w/v: 10% v/v) solution repeatedly until BSA was no longer detected in the supernatant. Finally, the products were washed with distilled water until the solution was neutral, and then dried in vacuum at 60 °C.

MHNTs@NIP was prepared as control by using the same procedure under the same conditions but without the template protein.

2.6 Adsorption experiments

Rebinding equilibrium and adsorption kinetics tests were performed to evaluate the recognition properties of MHNTs@BSA-MIP toward the template protein in batch mode operations.

For this purpose, 10 mg of MHNTs@BSA-MIP or MHNTs@NIP was immersed into a 10mL solution of BSA in PBS. The binding experiments were conducted in an incubator shaker at 25 °C for 24 h. After magnetic separation, the concentration of BSA in the supernatant was measured by a UV-vis spectrophotometer at 278 nm detection wavelength. The amount of protein adsorbed on the imprinted magnetic polymers was calculated based on the difference in BSA concentration before and after adsorption. All tests were conducted in triplicate.

The experimental data are presented as the adsorption capacity per unit mass (g) of MHNTs@BSA-MIP and the adsorption equilibrium capacity Q_e (mg/g) is calculated as follows:

$$Q_e = (C_o - C_e) \cdot V / m \quad (1)$$

Where C_o is the initial concentration of BSA solution (mg/L), C_e is the BSA concentration of the supernatant (mg/L), V is the volume of the initial solution (mL), and m is the amount of MHNTs@BSA-MIP or MHNTs@NIP(mg).

In the adsorption kinetics tests, 10 mg of MHNTs@BSA-MIP or MHNTs@NIP was added to 10 mL of BSA solution at an initial concentration of 200 mg/L and investigated at regular time intervals from 5-180 min at room temperature.

2.7 Selective adsorption experiments

The selectivity of MHNTs@BSA-MIP was evaluated at equilibrium adsorption condition using Lyz, OVA, and Try as competitive proteins. The competitive proteins were chosen according to their MW and pI. Both Lyz and Try have relatively smaller sizes than the BSA, and they have different pI values, i.e., 11.2 and 7.8, respectively. OVA have a smaller MW of 43 kDa and a similar pI of 4.7.

MHNTs@BSA-MIP or MHNTs@NIP (10 mg) was added to the mixture containing all of the proteins at a concentration of 200 mg/L and then incubated for 5 h. Then, the supernatants and polymers were separated by an external magnetic field, and the concentrations of proteins in the supernatant were measured by UV-vis spectrometry.

In addition, imprinting factor (*IF*) and selectivity coefficient (*SC*) were used to evaluate the selectivity property of MHNTs@BSA-MIP and MHNTs@NIP toward the template protein and competitive proteins. The *IF* and *SC* were calculated using the following equations:

$$IF = Q_{MIP} / Q_{NIP} \quad (2)$$

$$SC = IF_{TEM} / IF_{COM} \quad (3)$$

Where Q_{MIP} and Q_{NIP} (mg/g) represent the adsorption capacity of proteins for MHNTs@BSA-MIP and MHNTs@NIP, respectively, and IF_{TEM} and IF_{COM} are the *IF*s for the template protein and competitive proteins, respectively.

3 Results and discussion

3.1 Selection of monomers

In this work, MHNTs@BSA-MIP was prepared using NIPAM and MAA as co-monomers. The role of the monomer is to provide functional groups, which can form a complex with the template by covalent or non-covalent interactions. The strength of the interactions between template and monomer affects the affinity of MIP and determines the accuracy and selectivity of imprinted sites. The stronger the interactions is, the more stable the resultant complex prior to polymerization is, resulting in the better imprinting efficiency of the MIP, and therefore, correct selection of the functional monomers is of great importance. Given that BSA possesses more flexible conformational transitions in the imprinting process owing to its larger molecular size, hydrogen bonds between monomer NIPAM and BSA are too weak to form stable BSA-monomer complexes. To assist the imprinting of acid protein BSA (pI 4.9), an electrostatic interaction between monomer and BSA is considered, which is supposed to benefit the formation of imprinted sites in polymers. Therefore, MAA was chosen as additive monomer in BSA imprinting process owing to the strong electrostatic interactions of carboxyl groups toward amino groups of BSA. An appropriate mass of BIS was added to ensure the formation of stable protein-monomer complexes via multiple-point electrostatic interactions.

3.2 Preparation of MHNTs@BSA-MIP

The process for preparing a new kind of MHNTs@BSA-MIP was illustrated in Fig. 1, which combines the surface imprinting technique and a two-step immobilized template strategy. First, MHNTs were obtained according to a modified self-assembly coprecipitation method based on HNTs, and the surface Si-O-Si groups of MHNTs can be further modified through covalent attachment. MPS hydrolysis in toluene and its reaction with the Si-O-Si groups at the surface of the prepared MHNTs were allowed to proceed to synthesize MHNTs@C=C, whose surfaces comprise numerous vinyl groups. The addition of BIS

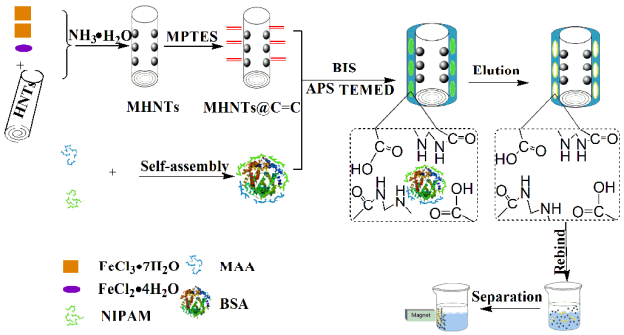

Fig. 1 Schematic representation of preparing MHNTs@BSA-MIP

as a cross-linker maintained the stability of the imprinting sites while facilitating easier handling and processing of the produced polymeric beads. Subsequently, BSA was selectively immobilized on the surface of the MHNTs@C=C through polymerization. After the removal of BSA, a thin polymer layer was obtained with imprinted cavities complementary to BSA in shape, size, and functional group orientation.

3.3 Characterization

3.3.1 TEM analysis

The morphological structures of HNTs (a), MHNTs (b), and MHNTS@BSA-MIP (c) were visualized using TEM in the Fig. 2. As shown in the Fig. 2a, the width of the HNTs was in the range of 30-60 nm and the inner diameter was 15-20 nm. In Fig. 2b, the Fe_3O_4 particles presented a calculated average size of 25 nm and then agglomerated on the surface of HNTs. In the TEM image of MHNTs@BSA-MIP, the polymer layer had
a thickness of approximately 15 nm, providing further evidence that the MIP grows through selective grafting on the exterior of MHNTs. The imprinted cavities on the surface of MHNTs@BSA-MIP can improve the mass transfer for adsorption of the template protein.

3.3.2 FT-IR spectra

The FT-IR spectra of MHNTs (a), MHNTs@C=C (b), and MHNTs@BSA-MIP (c) were shown in Fig. 3, which provided direct evidences for the synthetic process of MHNTs@BSA-MIP. As shown in Fig. 3a, the absorption peaks at 535 and 468 cm^{-1}

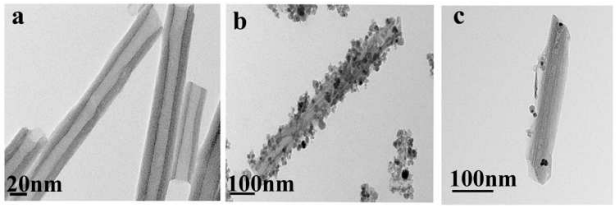

Fig. 2 TEM images of HNTs (a), MHNTs (b), and MHNTs@BSA-MIP(c)

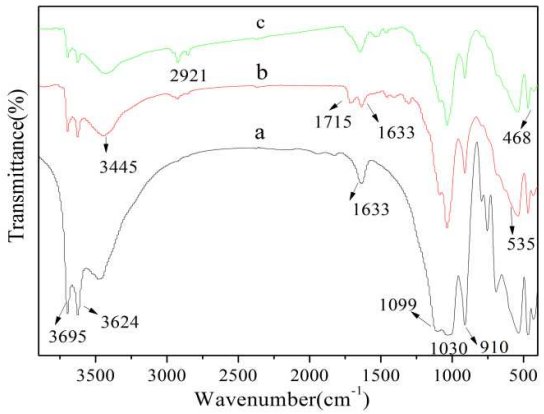

Fig. 3 FT-IR spectra of the MHNTs (a), MHNTs@C=C (b), and MHNTs@BSA-MIP (c)

belonged to the stretching of the Fe-O vibration for Fe_3O_4 nanoparticles, indicating the successful synthesis of MHNTs. The bands observed at 3695 and 3624 cm^{-1} denoted the stretching bands of hydroxyl group of HNTs. Interlayer water was indicated by the bending vibration at 1638 cm^{-1}. The peaks at 3445 and 1633 cm^{-1} were attributed to the characteristic absorptions of O-H stretching and C=C vibration of MHNTs, respectively. The characteristic peaks of Si-O-Si and deformation vibration of inner-surface hydroxyl groups for MHNTs (a), MHNTs@C=C (b), and MHNTs@BSA-MIP (c) were observed at around 1030 and 910 cm^{-1}, respectively. The peak at 1715 cm^{-1} for MHNTs@C=C indicated the successful functionalization with vinyl groups. The asymmetric stretching vibration of C-H of $-CH_2$ group at 2921 cm^{-1} showed that the imprinted polymer was successfully grafted on the surface of MHNTs@BSA-MIP.

3.3.3 XRD analysis

The XRD patterns of the synthesized Fe_3O_4 (a) and MHNTs@BSA-MIP (b) were shown in Fig. 4. In the 2θ range of

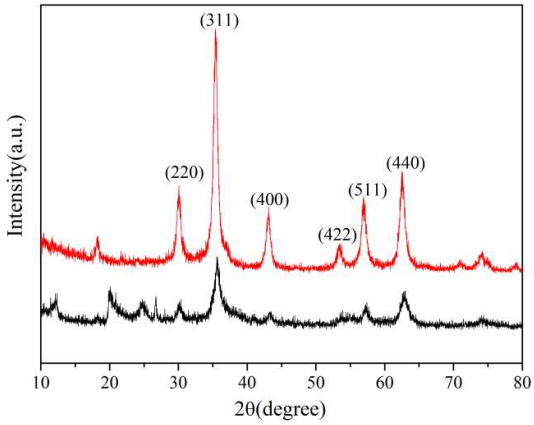

Fig. 4 XRD patterns of Fe_3O_4 (a), and MHNTs@BSA-MIP (b)

20°-70°, six characteristic peaks of Fe_3O_4 (2θ=30.25°, 35.56°,43.25°, 53.47°, 57.14°, 62.36°) were observed in the Fe_3O_4 and MHNTs@BSA-MIP. The peak positions could be indexed to (220), (311), (400), (422), (511), and (440), respectively, which matched well with the database of magnetite in the JCPDS-International Center for Diffraction Data (JCPDS Card: 19-629). The broad diffraction peak at 2θ=12°, 21°, 25° in MHNTs@BSA-MIP originated from the raw HNTs. These results may indicate that the Fe_3O_4 nanoparticles were actually embedded into the MHNTs. The XRD patterns showed that the synthesized particles contained Fe_3O_4, and the synthetic process did not change the phase of Fe_3O_4. Given that the crystal form of γ-Fe_2O_3 is similar to Fe_3O_4, XRD analysis cannot distinguish Fe_3O_4 from γ- Fe_2O_3. However, identifying the magnetic material is unnecessary because we are only concerned with their magnetic properties.

After precipitation polymerization with a crosslinking agent, the intensity of the XRD peaks decreased, which is attributed to the coating of the polymers on the MHNTs.

3.3.4 Magnetic properties of MHNTs and MHNTs@BSA-MIP

In the application of magnetic particles in fast separation, magnetic property was a crucial factor. In Fig. 5, the magnetic properties of the dried MHNTs (a) and MHNTs@BSA-MIP (b) at room temperature were investigated using VSM. The hysteresis loops showed no hysteresis, negligible coercivity, and remanence, which implied that the MHNTs and MHNTs@BSA-MIP had superparamagnetic properties. The saturation magnetization values obtained were 30 and 10 emu/g for MHNTs and MHNTs@BSA-MIP, respectively. Given that the extent of dipolar coupling is related to the distance between the particles, thus this characteristic depends on the thickness of the inert polymers layer. Fig. 5b strongly suggested that the remaining magnetic force in the

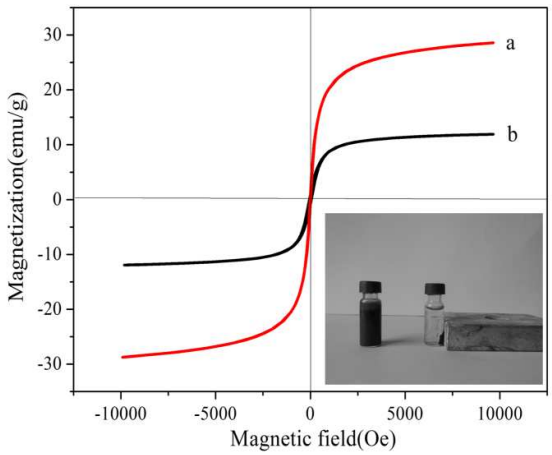

Fig. 5 The hysteresis loops of MHNTs (a), and MHNTs@BSA-MIP (b). The inset shows a photograph of the MHNTs@BSA-MIP dispersed in the water in the presence of an external magnetic field.

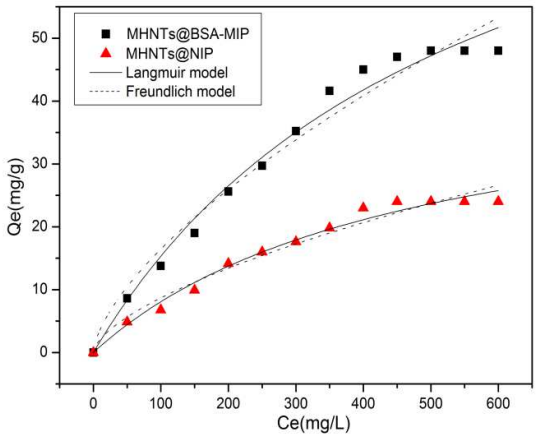

Fig. 6 Equilibrium adsorption of MHNTs@BSA-MIP (a), and MHNTs@NIP (b).

MHNTs@BSA-MIP could be attracted effectively and rapidly by an external magnetic field.

3.4 Adsorption properties of MHNTs@BSA-MIP

3.4.1 Adsorption isotherms

Adsorption isotherm curves were obtained to study the thermodynamic adsorption properties of the MHNTs@BSA-MIP. The Fig. 6 showed the rebinding capacities to BSA at different equilibrium concentrations with the temperature at 25 °C. Batch adsorption tests were performed at different initial concentrations of BSA, ranging from 50 mg/L to 600 mg/L, to compare the binding capacity of the MHNTs@BSA-MIP (a) against the MHNTs@NIP (b). The capacity of BSA onto the MHNTs@BSA-MIP increased rapidly with the increase of BSA concentration from 50 mg/L to 400 mg/L, and equilibrium was reached at 450 mg/L. Meanwhile, the adsorption capacity of MHNTs@BSA-MIP reached the value of 48.4 mg/g, and the adsorption capacity of NIP was 21.3 mg/g. This finding was probably due to binding of BSA to the MHNTs@BSA-MIP because of the specific binding to a limited number of binding sites in the polymers network, rather than the non-specific adsorption.

To evaluate the binding properties of MHNTs@BSA-MIP and MHNTs@NIP further, Langmuir and Freundlich models were selected to fit the experimental data according to the following equations:

$$\frac{C_e}{Q_e} = \frac{C_e}{Q_m} + \frac{1}{Q_m K_L} \quad (4)$$

$$Q_e = K_F C_e^{1/n} \quad (5)$$

Where Q_e is the equilibrium adsorption capacity (mg/g), C_e is the concentration of BSA in the final equilibrium solution (mg/L), and Q_m is the saturation capacity of the adsorbents (mg/g). K_L (L/mg) is the Langmuir adsorption constant, while K_F (mg/g) and *1/n* are the Freundlich adsorption equilibrium

Table 1

Adsorption isotherm constants for MHNTs@BSA-MIPand MHNTs@NIP

Adsorbent	Langmuir model			Freundlich model		
	K_L	Q_m	R	K_F	1/n	R
MHNTs@BSA-MIP	0.0018	98.34	0.9831	74.48	0.6557	0.9543
MHNTs@NIP	0.0021	45.81	0.9824	36.59	0.6246	0.9508

Table 2 Selectivity of the different prepared material in terms of *IF* (α) and *SC*

Adsorbents	supporter	*IF*				*SC*			Reference
		BSA	Lyz	OVA	Try	Lyz	OVA	Try	
Fe_3O_4@SiO_2@BSA-MIP	Fe_3O_4	1.70	1.27	1.12		1.34	1.52		[17]
MHNTs@BSA-MIP	MHNTs	2.27	1.08	1.11	1.30	2.10	2.05	1.75	This work

constants indicating the adsorption capacity and intensity, respectively.

Table 1 summarized the fitted parameters Q_m, K_L, K_F, *1/n*, and R^2 (correlation coefficient) and reveals that the Langmuir equation was found to better fit the isotherm data, with R^2 > 0.98.

3.4.2 Adsorption kinetics

Adsorption kinetics is important in evaluating adsorption efficiency. The Fig. 7 showed the relationship of the adsorption capacity of the MHNTs@BSA-MIP (MHNTs@NIP) and the adsorption time. Adsorption kinetics experiment was conducted using 200 mg/L of BSA onto the MHNTs@BSA-MIP at different time intervals as shown in Fig. 7a. Through MIP comparison between Fig. 7a and Fig. 7b, we found that the equilibrium adsorption of BSA on the MHNTs@BSA-MIP was approximately two times that of BSA on the MHNTs@NIP. MHNTs@BSA-MIP showed a rapid increase in the first 40 min, achieving 90% of the equilibrium adsorption capacity. Then, the adsorption rate slowly increased with time. We can speculate that a large number of imprinted cavities existed on the surface of the MHNTs@BSA-MIP, making the template protein accessible to the specific binding sites at an early time. In time, more and more imprinted cavities were filled up, space steric hindrance became bigger, and the diffusion of template protein into the molecular imprinted cavities became slower. Finally, the molecularly imprinted cavities were fully occupied and adsorption reached equilibrium. For the MHNTs@NIP, no imprinted cavity was found, and the low adsorption capacity to template protein was attributed to nonspecific adsorption. The results in this rebinding process were in agreement with those in the common adsorption process.

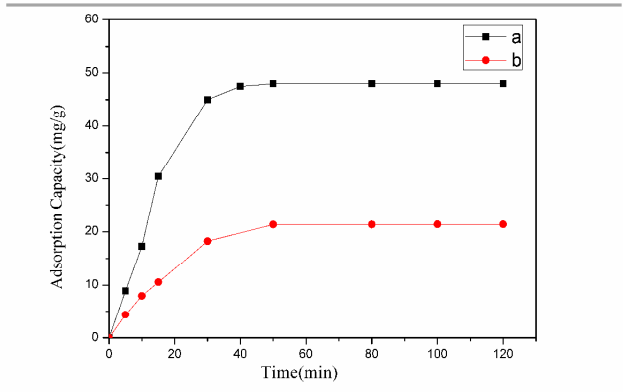

Fig. 7 Dynamic adsorption of MHNTs@BSA-MIP (a), and MHNTs@NIP (b)

3.4.3 Adsorption specificity

The adsorption capacities and selectivity factors of the MHNTs@BSA-MIP and MHNTs@NIP for different proteins in PBS with a feed concentration of 200 mg/L was presented in Fig. 8. Lyz, OVA, and Try were chosen as competitive proteins in the selectivity adsorption experiments. The choice of competitive proteins was based on their MW and pI. Compared with the template BSA, OVA has a similar pI of 4.7 and has a smaller size. Both Lyz and Try have relatively smaller sizes than BSA, while they have different pI values, i.e., of 11.2

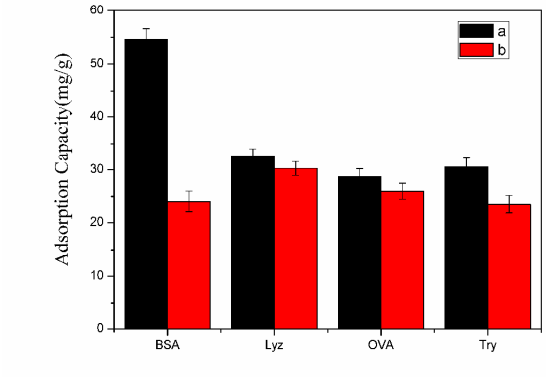

Fig. 8 Selectivity adsorption of MHNTs@BSA-MIP (a) and MHNTs@NIP(b)

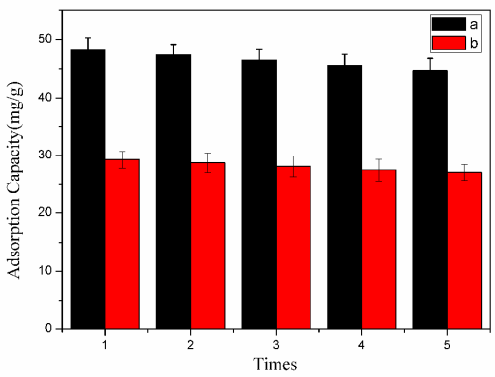

Fig. 9 The stability and regeneration of MHNTs@BSA-MIP (a) and MHNTs@NIP (b)

and 7.8, respectively.

The selectivity of the MHNTs@BSA-MIP in terms of *IF* (α) and *SC* was compared with other work. The results were listed in Table 2. The MHNTs@BSA-MIP exhibited much higher absorptive capacity and *IF* for BSA than for the competitive proteins as shown in Table 2. On one hand, for the competitive proteins, no strong shape memory effects to enter into the imprinted cavities were found because they are much smaller than the imprinted cavities produced by BSA. On the other hand, they have different pI values from the template BSA. Thus, the microenvironment of binding process was unsuitable for the competitive proteins. The shape memory effect and multiple non-covalent interactions complementary to template protein in the form of electrostatic interaction, hydrogen bonding, and hydrophobic interaction play important roles in protein recognition in the MHNTs@BSA-MIP.

3.5 Regeneration and reproducibility

Regeneration and reusability is one of the most important properties for the application of MHNTs@BSA-MIP. The adsorption-desorption cycles were repeated for several times for the same batch of MIP to verify their regeneration and reusability. The MHNTs@BSA-MIP after BSA absorption was washed with an SDS-acetic acid (10% w/v: 10% v/v) solution to remove BSA and applied to rebind BSA. As shown in Fig. 9, the adsorption capacity for BSA showed only a slight decrease after continuous adsorption and desorption processes, whereas the adsorption capacity of MHNTs@NIP toward BSA remained unchanged. This finding could be attributed to changes in special recognition sites that are sterically complementary to BSA caused by repeated washing. However, given that the MHNTs@NIP had no special recognition sites, the affinity of MHNTs@NIP was nonspecific, and the effect of washing was negligible. The data confirmed that the MHNTs@BSA-MIP has an outstanding reusability.

4 Conclusion

In this work, a facile procedure for preparation of MHNTs@BSA-MIP was developed by combining a surface imprinting technique and magnetic separation technology for selective recognition of BSA. Attachment of Fe_3O_4 on the surface of HNTs was achieved by coprecipitation method, which occurred in the presence of two ferric salts and pure HNTs. The MHNTs@BSA-MIP was prepared using modified MHNTs as support. The MHNTs@BSA-MIP demonstrated saturation magnetization, rapid dynamic adsorption, high adsorption ability, and a higher reusability for adsorption of the template protein than the MHNTs@NIP. Separation was easily done by using an external magnetic field. The MHNTs@BSA-MIP exhibited potential application in protein separation, solid-phase extraction, chromatographic separation, drug delivery, and medical diagnostics.

More detailed investigation on enhancing the imprinting efficiency in terms of *IF* and specific rebinding capacity should be conducted. Follow-up work and appropriate measures should be performed to adjust the thickness and composition of MIP. For example, the amount of functional monomers with stronger specific adsorption for the template molecule may be increased or varied to improve *IF*.

Acknowledgement

The authors greatly acknowledge the financial support from National Natural Science Foundation of China (21276283).

References

1 E. Ueda, P. Gout and L. Morganti, *J. Chromatogr. A* 2003, 988, 1-23.
2 J. A. Asenjo and B. A. Andrews, *J. Chromatogr. A*, 2012, 1238, 1-10.
3 P. G. Righetti, R. Sebastiano and A. Citterio, *Proteomics*, 2013, 13, 325-340.
4 X. Jia, M. Xu, Y. Wang, D. Ran, S. Yang and M. Zhang, *Analyst*, 2013, 138, 651-658.
5 A. Poma, A. Guerreiro, S. Caygill, E. Moczko and S. Piletsky,

RSC Adv., 2014, 4, 4203-4206.
6 J. Pan, W. Zhu, X. Dai, X. Yan, M. Gan, L. Li, H. Hang and Y. Yan, *RSC Adv.,* 2014, 4, 4435-4443.
7 S. Zhong, Y. Kong, L. Zhou, C. Zhou, X. Zhang and Y. Wang, J. *Chromatogr.B,* 2014, 945-946, 39-45.
8 E. Verheyen, J. P. Schillemans, M. van Wijk, M.-A. Demeniex, W. E. Hennink and C. F. van Nostrum, *Biomaterials*, 2011, 32, 3008-3020.
9 J. Liu, K. Yang, Q. Deng, Q. Li, L. Zhang, Z. Liang and Y. Zhang, *Chem. Commun.* , 2011, 47, 3969-3971.
10 H. Chen, J. Kong, D. Yuan and G. Fu, *Biosens. Bioelectron.*, 2014, 53, 5-11.
11 Y.-Q. Yang, X.-W. He, Y.-Z. Wang, W.-Y. Li and Y.-K. Zhang, *Biosens. Bioelectron.*, 2014, 54, 266-272.
12 M. E. Çorman, C. Armutcu, L. Uzun, R. Say and A. Denizli, *Colloids Surf., B*, 2014, 123, 831-837.
13 D.-Y. Li, Y.-P. Qin, H.-Y. Li, X.-W. He, W.-Y. Li and Y.-K. Zhang, *Biosens. Bioelectron.*, 2015, 66, 224-230.
14 G. Pan, Q. Guo, C. Cao, H. Yang and B. Li, *Soft Matter*, 2013, 9, 3840-3850.
15 M. Zhang, Y. Wang, X. Jia, M. He, M. Xu, S. Yang and C. Zhang, *Talanta*, 2014, 120, 376-385.
16 K. Zhao, B. Lin, W. Cui, L. Feng, T. Chen and J. Wei, *Talanta*, 2014, 121, 256-262.
17 X. Li, B. Zhang, W. Li, X. Lei, X. Fan, L. Tian, H. Zhang and Q. Zhang, *Biosens. Bioelectron.*, 2014, 51, 261-267.
18 R. Gao, X. Mu, Y. Hao, L. Zhang, J. Zhang and Y. Tang, J. *Mater. Chem. B*, 2014, 2, 1733-1741.
19 H. Guo, D. Yuan and G. Fu, *J.Colloid Interface Sci,* 2015, 440, 53-59.
20 H. He, G. Fu, Y. Wang, Z. Chai, Y. Jiang and Z. Chen, *Biosens. Bioelectron.*, 2010, 26, 760-765.
21 R. Ouyang, J. Lei and H. Ju, *Chem Commun*, 2008, 5761-5763.
22 G. Fu, H. He, Z. Chai, H. Chen, J. Kong, Y. Wang and Y. Jiang, *Anal.Chem.*, 2011, 83, 1431-1436.
23 Z. Lin, Z. Xia, J. Zheng, D. Zheng, L. Zhang, H. Yang and G. Chen, *J. Mater. Chem.*, 2012, 22, 17914-17922.
24 X. Hu, L. Xie, J. Guo, H. Li, X. Jiang, Y. Zhang and S. Shi, *Food Chem.*, 2015, 179, 206-212.
25 D. Zhu, Z. Chen, K. Zhao, B. Kan, H. Li, X. Zhang, B. Lin and L. Zhang, *RSC Adv*., 2015, 5, 26977-26984.
26 L. Yuan, L. Jiang, T. Hui, L. Jie, X. Bingbin, Y. Feng and L. Yingchun, *Sens. Actuators, B*, 2015, 206, 647-652.
27 H. Duan, L. Li, X. Wang, Y. Wang, J. Li and C. Luo, *RSC Adv.*, 2015, 5, 18850-18857.
28 R. Gao, Y. Hao, X. Cui, L. Zhang, D. Liu and Y. Tang, *J. Alloys Compd*., 2015, 637, 461-465.
29 S. Xu, H. Lu, L. Chen and X. Wang, *RSC Adv.*, 2014, 4, 45266-45274.
30 H.-J. Chen, Z.-H. Zhang, L.-J. Luo and S.-Z. Yao, *Sens. Actuators*, B, 2012, 163, 76-83.
31 J. Huang, X. Xing, X. Zhang, X. He, Q. Lin, W. Lian and H. Zhu, *Food Res. Int.*, 2011, 44, 276-281.
32 W. O. Yah, H. Xu, H. Soejima, W. Ma, Y. Lvov and A. Takahara, *J. Am.Chem. Soc.*, 2012, 134, 12134-12137.
33 W. O. Yah, A. Takahara and Y. M. Lvov, *J. Am. Chem. Soc.*, 2012, 134, 1853-1859.
34 C. Zhou, H. Li, H. Zhou, H. Wang, P. Yang and S. Zhong, *J. Sep. Sci.*, 2015, 38, 1365-1371.
35 J. Pan, B. Wang, J. Dai, X. Dai, H. Hang, H. Ou and Y. Yan, *J. Mater. Chem.*, 2012, 22, 3360.
36 J. Dai, X. Wei, Z. Cao, Z. Zhou, P. Yu, J. Pan, T. Zou, C. Li and Y. Yan, *RSC Adv.*, 2014, 4, 7967.
37 J. Pan, H. Yao, L. Xu, H. Ou, P. Huo, X. Li and Y. Yan, *J. Phys. Chem.*, 2011, 115, 5440-5449.
38 S. Zhong, C. Zhou, X. Zhang, H. Zhou, H. Li, X. Zhu and Y. Wang, *J. Hazard. Mater.*, 2014, 276, 58-65.